Desalination and Water Treatment
www.deswater.com

doi: 10.5004/dwt.2021.27348

228 (2021) 176–186
July

Control of an electronic ballast-discharge lamp system supplied by a multicellular converter dedicated to water purification

Aicha Aissa Bokhtache[a,b], Abdallah Zegaoui[a,b], Rachid Taleb[a,*], Michel Aillerie[b]

[a]*Electrical Engineering Department, Laboratoire Génie Electrique et Energies Renouvelables (LGEER), Hassiba Benbouali University of Chlef, Algeria, emails: r.taleb@univ-chlef.dz (R. Taleb), a.aissabokhtache@gmail.com (A.A. Bokhtache), a.zegaoui@univ-chlef.dz (A. Zegaoui)*
[b]*Laboratoire Matériaux Optiques, Photonique et Systèmes (LMOPS), University of Lorraine, Metz, France, email: aillerie@metz.supelec.fr*

Received 27 September 2020; Accepted 12 April 2021

ABSTRACT

The presence of pathogenic microorganisms in water presents a health risk for consumers of all ages. Ultraviolet (UV) sterilization system is recommended by health services thanks to the fact that UV radiation has fast action, efficient, safe and is an economic process that respects the environment. In recent years, high-frequency electronic ballasts for discharge lamps were presented as a substitute for magnetic ballast. In the aim of generation a maximum of UV radiation at 253.7 nm (germicidal effect), it is necessary to optimize its power supply with a sinusoidal current at high-frequency, generally, about 50 kHz and arms value adapted to the lamp. We present in this contribution, the design of a high-frequency power supply (electronic ballast) based on a multicellular converter operating as an inverter. Compared to standard power supplies, the advantage of this topology is the reduction of the blocking voltage stress on the switches. Starting with the model of a converter operating in an open loop, we introduce a PI control allowing a significant improvement of the waveforms of voltage and arc current of the discharge lamp. By else, the water temperature, in which the lamp is submerged, influences the pressure of the mercury atoms in the lamp and consequently the emission of the desired ray. Then, in this contribution, we test the robustness of the controller and show that the topology of the power supply based on a multicellular converter associated with the PI control is a powerful solution to initiate the discharge and to optimize the emission of a UV-C lamp dedicated for water purification.

Keywords: Low-pressure mercury-argon discharge; Germicide; UV-C lamp; Electronic ballast; Pulse Width Modulation; Modulating duty cycles control; Multicellular converter

1. Introduction

Consuming water with no risk to health is a basic need for all mankind. Everywhere in the world, water is contaminated with toxic substances such as pesticides, hormones or microorganisms that can be harmful to humans [1]. The disinfection of water is essential for sanitary safety and for minimizing the risk of infection by pathogenic microorganisms allowing preventing the spread of waterborne diseases [2].

Because they are difficult to implement, conventional chemical treatments are generally not a good method as they have the double disadvantages of misrepresenting the organoleptic qualities of water and rejecting of polluted water [3]. A second possible method is based on UV disinfection, especially interesting when it is associated with a pre-filter [4]. UV sterilization system is recommended in health services because UV radiation has fast action, efficient, safe and is an economic process that respects the environment. This technique is currently used in developed nations and in many Mediterranean countries [5].

* Corresponding author.

In recent years and nowadays, high-frequency electronic ballasts for gas discharge lamps have been presented as a substitute for the magnetic ballast. This evolution of technology is due to the best qualities achieved by electronic ballast as high power factor, high electrical to photon conversion efficiency, best possible control of lighting with no blinking and no electromagnetic noise, and finally advantageous size and weight and longer mean time before failure (MTBF) [6,7]. Therefore, for all these reasons, special attention should be accorded to electronic ballasts consisting in the optimization of the power supply of the ballast in order to generate a maximum of UV-C radiation at exactly 253.7 nm for which the germicidal effect is maximum [8,9]. To recall, the UV range is divided in three bands shown in Table 1.

In previous studies, Aissa-Bokhtache et al. [9,10] demonstrated the relevance of using fuzzy control in a conventional converter delivering at its output terminals a 50 kHz sinusoidal current of 0.65 arms for supplying a low-pressure discharge lamp-electronic ballast system dedicated to water purification and therefore emitting a maximum of UV radiation at 253.7 nm. Within fuzzy technique control, this converter delivers output sinusoidal current and voltage with Total Harmonic Distortion (THD) equal to 5.58% and 4.49% respectively associated with a good robustness to disturbances up to ±60%.

In the current work, we present a new electrical current source based on a multicellular converter to supply the same type of discharge lamp as previously considered. The main aim of this study is the improvement of the current waveform, the THD, as well as the robustness of the whole system. It is to be noted that this kind of converter is mainly dedicated to the distribution of the voltage stress on power switches in high power supplies. To our knowledge in literature, this multicellular converter was never used to supply discharge lamp-electronic ballast system and even, never consider for that purpose. With all the possible advantages of this topology of the converter as mentioned above, then we can expect for supplying discharge lamp, we introduce this kind of converter for water purification system. Special attention is given to the study of the efficiency of the overall system composed by the set power-supply/electronic-ballast/discharge-lamp at 253.7 nm.

We started the simulation of the system operating in an open-loop configuration. After introducing a proportional-integral regulator, we performed all robustness tests for the system operating in a closed loop. During this study, the electric model of the lamp validated by [9,10] was considered. The performances of this new power-supply/electronic-ballast/discharge-lamp setup were analyzed considering the various electrical output characteristics, arc currents and voltages and their THD, and the response and robustness of the system.

Table 1
Spectrum highlighting UV-A, UV-B and UV-C

Name	Abbreviation	Wavelength range
Ultraviolet A	UV-A	400–315 nm
Ultraviolet B	UV-B	315–280 nm
Ultraviolet C	UV-C	280–100 nm

2. Modeling of a discharge lamp-electronic ballast system

The studied power-supply/electronic-ballast/discharge-lamp setup is represented in Fig. 1.

We can see in the photo of Fig. 1 the disinfection chamber, which crosses the water, also integrating the lamp, the power supply and the electronic ballast. In the chamber, microorganisms are exposed to intense ultraviolet light. This has for consequences a damage of their genetic molecules, that is, nucleic acids: DNA and RNA, inducing the inactivation of the microorganisms by blocking the reproduction process and thus, avoiding a possible following infection in human or animal hosts.

Ballast supplies the UV lamp and controls its power. It must operate at a temperature below 60°C to prevent its premature failure. The type of ballasts most frequently used is the electronic or electromagnetic ones. Electronic ballasts, which operate at very high-frequency, have lower consumption and best efficiency due to lower heating than electromagnetic ballasts [6,7]. By else, due to a constant power output at a nominal constant frequency, electronic ballasts present a higher MTBF [12].

2.1. Discharge-lamp

Low-pressure mercury vapor lamps emit a quasi-monochromatic light at 253.7 nm, which corresponds to the optimum band of the germicidal effect. They have the form of long tubes of 1.5 to 2 cm in diameter. Standard lengths of tube are 91.4 and 162.6 cm for arc lengths of 76.2 and 147.3 cm respectively [11]. Low-pressure lamps possess a MTBF of about 3,500 h. The lamps are usually inserted inside a quartz sleeve, which allows direct immersion into the water to be treated. Quartz transmits up to 90% of the radiation coming from the lamp. The transmitted light intensity depends on the power, the temperature of the lamp and water, and the degree of fouling. Mercury vapor lamps are very sensitive to temperature variations. Very low temperature causes a drop in pressure and the mercury atoms are thereby less compressed and more difficult to excite causing a decrease in transformed energy quantity. Conversely, an increase in temperature increases the pressure, the electron excitation of mercury atoms is very large but light energy will be released in a much broader spectrum than

Fig. 1. Schematic of UV unit with cover removed [11].

253.7 nm. Finally, the optimum UV emission is achieved when its temperature is around 50°C [12]. This analysis of the functioning of a lamp points out the necessity to drive the lamp with an optimized controller presenting a high level of regulation and robustness. In addition, with respect to the load, the power supply is a generator acting as a current source generally a ballast constituting an inductive impedance. In [12,13], Costach et al. selected the supply voltage twice the arc voltage to assume an operating point around a low arc current.

The considered UV-C lamp is manufactured by the company Philips® (France). Fig. 2 shows the discharge lamp model where R_{arc} is a resistor depending of both arc power and arc temperature of the lamp and where r_f is related to each cathode filament [14–17]. The lamp characteristics are summarized in Table 2.

In the following, the index "arc", "lamp", and "load" correspond to the arc, the lamp, and the load respectively in the notation of the voltages, the intensities and the powers. The model is described by Eqs. (1)–(3).

The lamp voltage, V_{lamp} is given as follows:

$$\overrightarrow{V_{lamp}} = \left[\left(1+\frac{rf^2}{rf^2+Z_{Cp}^2}\right)V_{arc} + rf\times\frac{P_{arc}}{V_{arc}}\right] + j\frac{rf\times Z_{Cp}}{rf^2+Z_{Cp}^2}V_{arc} \quad (1)$$

and the resonant load current i_{Load} is the sum of the arc current and filament current:

$$\overrightarrow{i_{Load}} = \vec{i}_{arc} + \vec{i}_{Cp} = \left(i_{arc}+\frac{rf}{rf^2+Z_{Cp}^2}\right)V_{arc} + j\frac{Z_{Cp}}{rf^2+Z_{Cp}^2}V_{arc} \quad (2)$$

where i_{Cp} is the current through the parallel capacitor C_p and Z_{Cp} is C_p reactance, and L_r and C_r are the resonant circuit elements.

Table 2
Equivalent circuit parameters of the lamp

V_{arceff}	111 V	r_f	5 Ω
I_{arceff}	0.65 A	P	65 W
R_{arc}	170.769 Ω	L_{tube}	150 cm

The total power of the lamp is obtained by:

$$P_{lamp} = \mathrm{Re}\left[\overrightarrow{V_{lamp}}\times\vec{i}_r\right] = \frac{2rf^3}{rf^2+Z_{Cp}^2}V_{arc}^2 + \left(1+\frac{2rf^2}{rf^2+Z_{Cp}^2}\right)P_{arc} + rf\left(\frac{P_{arc}}{V_{arc}}\right) \quad (3)$$

and finally, using the Laplace operator, the transfer function can be achieved using the design of a conventional current divider to the electrical circuit (Fig. 2).

$$\frac{I_{arc}}{V_{Load}} = \frac{rfC_rC_ps^2 + C_rs}{\left(R_{arc}+rf\right)L_rC_rC_ps^3\left[\left(2R_{arc}+rf\right)L_rC_rC_p + L_rC_r\right]s^2 + \left(R_{arc}+rf\right)\left(C_r+C_p\right)s+1} \quad (4)$$

2.2. Multicellular-converter

As shown in Fig. 3, the principle of a multicellular-converter is based on the series connection of switching cells in order to divide the total voltage at each cell and thus to share the stresses voltage on multiple semiconductor components [18]. This technique allows keeping power switches under supportable voltage magnitudes in both ON and OFF states. Multiplying the number of intermediate cells reduces the amplitude of each rising or falling edge of the inverter output voltage. Thus, the amplitude of harmonics is even low [19,20]. Therefore, each cell is composed by two power switches in push-pull topology and connected to other cells by a flying capacitor.

In our case, inverter structure is composed of $P = 4$ switch cells, separated from each other by $P - 1 = 3$ flying capacitors. This induces at the output of the inverter $P + 1 = 5$ voltage levels allowing to achieve a signal with a shape relatively close to a pure ac signal, that is, with a satisfactory small total harmonic distortion [19,20]. It is to be noted that the use of pulse width modulation, as in our system, will eliminate some residual harmonic lines families. In addition to these two major advantages, multicellular converter avoids switches being in short-circuit that is the most common failure appearing in converters. Nevertheless, the effective consideration of this property requires a suitable choice of structural components for a rapid detection of isolation fault and a reconfiguration

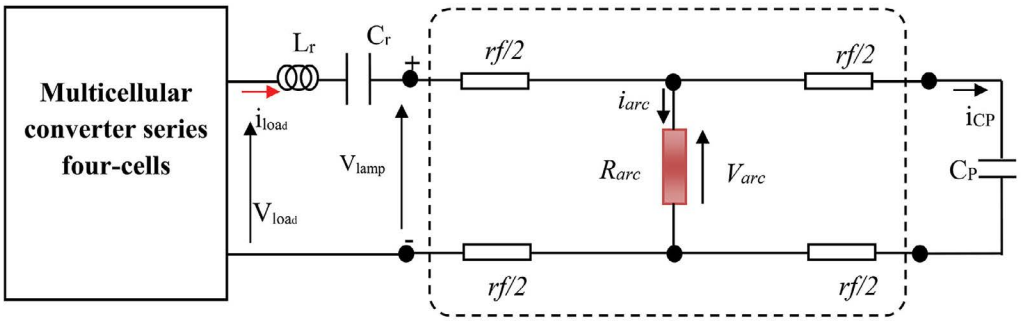

Fig. 2. Equivalent circuit of the electronic ballast-discharge lamp with multi cellular-serial converter four-cell.

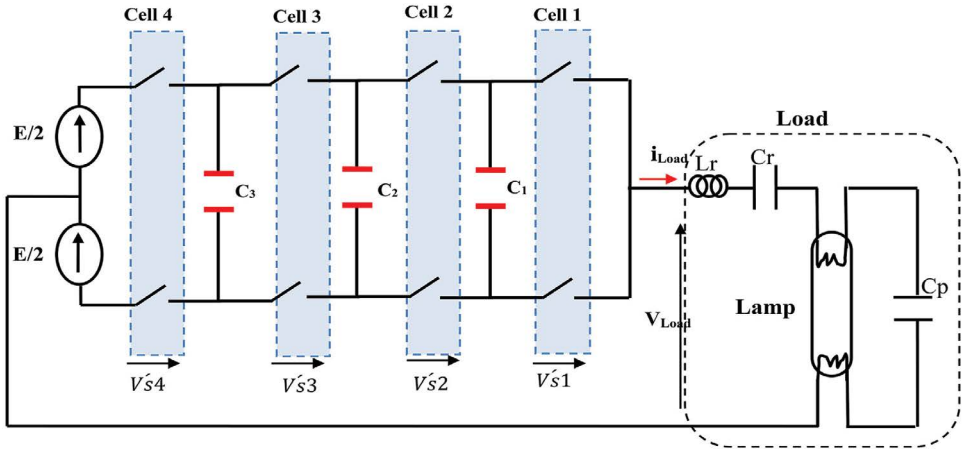

Fig. 3. Five levels multicellular inverter (four switch cells in series) [23].

of the remaining healthy cells for a possible operation in degraded mode [21,22].

We use MOSFET switches well adapted for low and medium power applications (less than a few tens of kilowatts). It is often used in low voltage supply applications with switching frequencies less than100 kHz [23].

By using instantaneous model of the multicellular converter, KCL allows us to write the voltage equation across the load:

$$V_{\text{Load}} = \sum_{k=1}^{p} V'_{\text{Sk}} - \frac{E}{2} \tag{5}$$

$$V_{\text{Load}} = \left(u_1 - u_2\right)V_{c1} + \left(u_2 - u_3\right)V_{c2} + \cdots + \left(u_{p-1} - u_p\right)V_{\text{cp}-1} + u_p \cdot E - \frac{E}{2} \tag{6}$$

In the following, for clarity and to be in agreement with the specific application that we have developed, we consider the $P = 4$, even if a generalization of the proposed system can be easily achieved.

Thus, with 3 capacitors, we can write:

$$\begin{cases} \dfrac{dV_{c1}}{dt} = \dfrac{1}{C_1}\left(u_2 - u_1\right)i_{\text{Load}} \\ \dfrac{dV_{c2}}{dt} = \dfrac{1}{C_2}\left(u_3 - u_2\right)i_{\text{Load}} \\ \dfrac{dV_{c3}}{dt} = \dfrac{1}{C_3}\left(u_3 - u_2\right)i_{\text{Load}} \\ V_{\text{Load}} = \left(u_1 - u_2\right)V_{c1} + \left(u_2 - u_3\right)V_{c2} + \left(u_3 - u_4\right)V_{c3} + u_4 \cdot E - \dfrac{E}{2} \end{cases} \tag{7}$$

where V_{Load} and i_{Load} are respectively the voltage and the current across the system discharge lamp-electronic ballast, V_{ck} is the voltage across each flying capacitor k, u_k is the control order (1 or 0), C_k are the flying capacitors and V'_{sk} is the voltage across the switch.

2.3. Pulse Width Modulation modulation technique

For controlling the cells of the inverter, the natural Pulse Width Modulation (PWM) technique is generally used. It is a well-known simple technique easier to implement [24]. For optimal operation, command signals must be mutually phased shifting by $2\pi/P$. In natural PWM, intersection between a f_p frequency triangular carrier and the modulating sinusoidal signal f_{mod} frequency generates the control signal for each cell.

Considering the triangular signals noted p_k in the interval [0,1], the following equations respect the mathematical model:

$$P_k = \frac{1}{2}\left[\frac{2}{\pi} \cdot \arcsin\left[\sin\left(2 \cdot \frac{\pi}{P} \cdot t - \Phi_k + \frac{\pi}{2}\right)\right] + 1\right] \tag{8}$$

$$\begin{cases} P_1 = \dfrac{1}{2}\left[\dfrac{2}{\pi} \cdot \arcsin\left[\sin\left(2 \cdot \pi \cdot f_p \cdot t - \Phi_1 + \dfrac{\pi}{2}\right)\right] + 1\right] \\ P_2 = \dfrac{1}{2}\left[\dfrac{2}{\pi} \cdot \arcsin\left[\sin\left(2 \cdot \pi \cdot f_p \cdot t - \Phi_2 + \dfrac{\pi}{2}\right)\right] + 1\right] \\ P_3 = \dfrac{1}{2}\left[\dfrac{2}{\pi} \cdot \arcsin\left[\sin\left(2 \cdot \pi \cdot f_p \cdot t - \Phi_3 + \dfrac{\pi}{2}\right)\right] + 1\right] \\ P_4 = \dfrac{1}{2}\left[\dfrac{2}{\pi} \cdot \arcsin\left[\sin\left(2 \cdot \pi \cdot f_p \cdot t - \Phi_4 + \dfrac{\pi}{2}\right)\right] + 1\right] \end{cases} \tag{9}$$

The angle Φ_k will be chosen equal to $\Phi_k = (k - 1)\cdot 2\pi/P$, where P is the number of cells. Comparison between triangular signal p_k and the modulating one mod_k, allows us to obtain the control signals u_k.

The control signals are obtained by pulse width modulation PWM by the natural technique and modulating mod_k is sinusoidal.

$$\text{mod}_k = r \cdot \sin\left(2 \cdot \pi \cdot f_{\text{mod}} \cdot t\right) \tag{10}$$

With r represents the modulation depth of between 0 and 1.

The choice of a regular shifting phase of $2\pi/P$ between the different cells improves significantly the spectrum quality of the output voltage [24]. Thus we find that harmonics are gathered in families centered on multiple frequencies $p.m.f_{mod}$, where $m = f_p/f_{mod}$ is the modulation index.

To assume a constant voltage at the capacitors' terminals, we generally add to the system a controller allowing a closed-loop control of the duty cycles. This controller assumes a modulation of the duty cycles that reflects the conduction periods of the different power switches. The global system is thus represented in Fig. 4.

The new modulating signals, $D_1 - D_4$, generated by the controller in close-loop are sinusoidal and given by the following formula:

$$D_k = D_{k+1} - G \cdot \text{sign}\left(i_{\text{Load}}\right) \cdot \left(\frac{C_k}{T_{\text{dec}} \cdot i_{\text{Load}}}\right) \cdot \left(\frac{k \cdot E}{p} - V_{\text{ck}}\right) \tag{11}$$

where D_k, D_{k+1} are the duty cycles of cells k and $k + 1$ and sign (i_{Load}) represents the sign of i_{Load}.

From Eq. (11) we see that the load current weighted by the proportional gain corresponds to the average value i_{Load}. Fig. 4 presents the structure of the modulating control duty cycle's generation with the considered inverter, the control law must take into account the sign of the sinusoidal load current [25].

We note that there are p control values (p duty cycles) and ($p - 1$) flying capacitor voltages to control. This implies that the additional control value will be constant selected according to the operating point.

D_4 (duty cycle of the cell connected to the voltage source E) was chosen. In this regulation, we use a reference signal expressed by:

$$D_{\text{ref}} = r \cdot \sin\left(2 \cdot \text{pi} \cdot f_{\text{mod}} \cdot t\right) + \frac{1}{2} = D_4 \tag{12}$$

where $\alpha_k = D_{k+1} - D_k$. If $D_k \geq P_k$ then $u_k = 1$, and if $D_k \leq p_k$ then $u_k = 0$.

The choice of the gain G is performed in a manner to ensure a non-saturation control variables and a maximum dynamic [24–26].

During the starting time of the converter within zero-voltage, the previous equations allow us to obtain the gain G as follow:

$$G = \frac{T_{\text{dec}} \cdot I_{\text{Loadmax}}}{C_k \cdot (p-1) \cdot E} \tag{13}$$

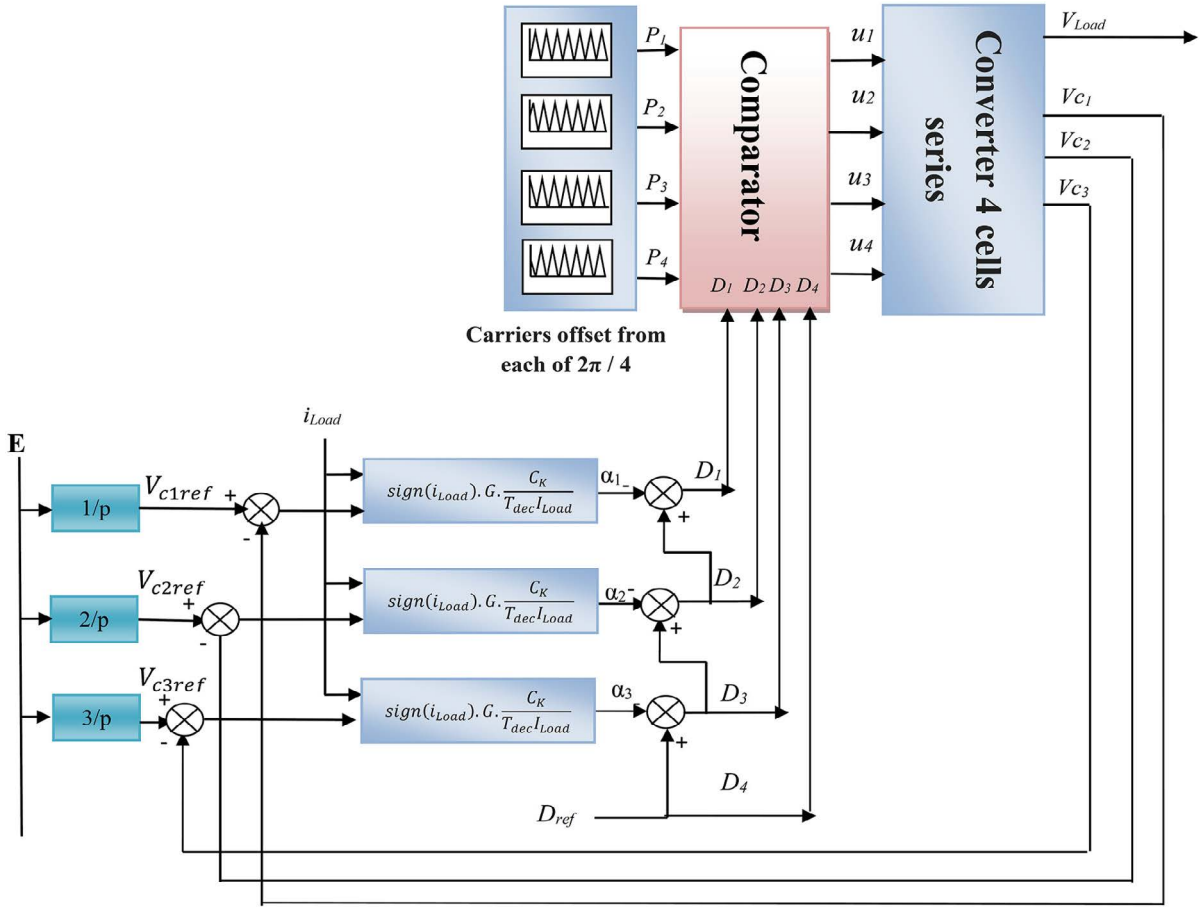

Fig. 4. Structure of the modulating control duty cycles law [24,25].

As we have modeled all the elements of the system, that is, the lamp, Eq. (4), the multi-cellular converter Eq. (5), and the PWM driving system with the associated duty-cycles controllers, Eqs. (6)–(13), the functioning simulation can be now performed. The main simulation results pointing out the high performances of this original power supply of UV lamp for water purification are presented in the following paragraphs.

The simulation was done under the MATLAB-sim PowerSystems environment. The functioning characteristics of the converter are summarized in Table 3. The considered parameters are E the supply voltage, C_1, C_2 and C_3, the flying capacitors; f_{dec} the switching frequency f_{mod} the frequency of the modulating and r is the modulating ratio varying between 0 and 1.

2.4. Simulation of the discharge lamp-electronic ballast system in open-loop

We present in the two following Figs. 5 and 6, the main characteristics of the voltages and currents of the load and of the capacitors of the inverter.

Table 3
Multicellular converter features

Voltage supply	800 V
$C_1 = C_2 = C_3 = 5$nF	0.65 A
f_{dec}	3.2 MHz
f_{mod}	50,000 Hz
Modulation ratio r	0.472

Fig. 5 shows that the voltages across flying capacitors achieved a constant level corresponding to $k \times E/P$, after a transient initial stage link to the time constant of the global system.

We also report in Figs. 6 and 7, the currents of voltages, and their corresponding harmonic spectra, of the load and arc, respectively.

Due to the high stability of the flying capacitor voltages, we can notice that the load current (Fig. 6a) is a sinusoidal signal of 50 kHz and that the converter output voltage (Fig. 6b) follows the five intermediate levels ($-E/4$, $-E/2$, 0, $E/4$, $E/2$) defined by Eq. (5). The THD of the load current was measured equal to 0.27%. We also report in Fig. 7 the waveform of the arc voltage and current. The quality of the delivered current and voltage to the lamp achieves a satisfactory functioning point of the lamp allowing it to emits the expected quasi-monochromatic light at 253.7 nm, for an optimum germicidal effect.

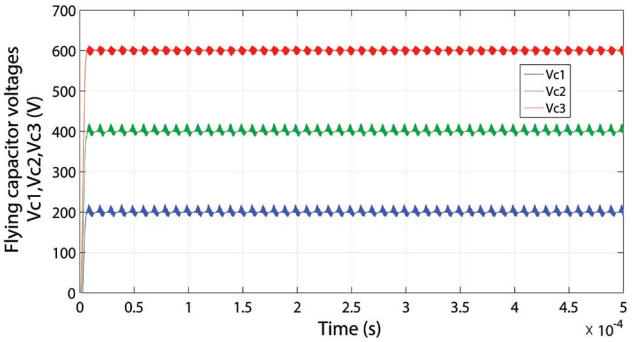

Fig. 5. Flying capacitor voltages.

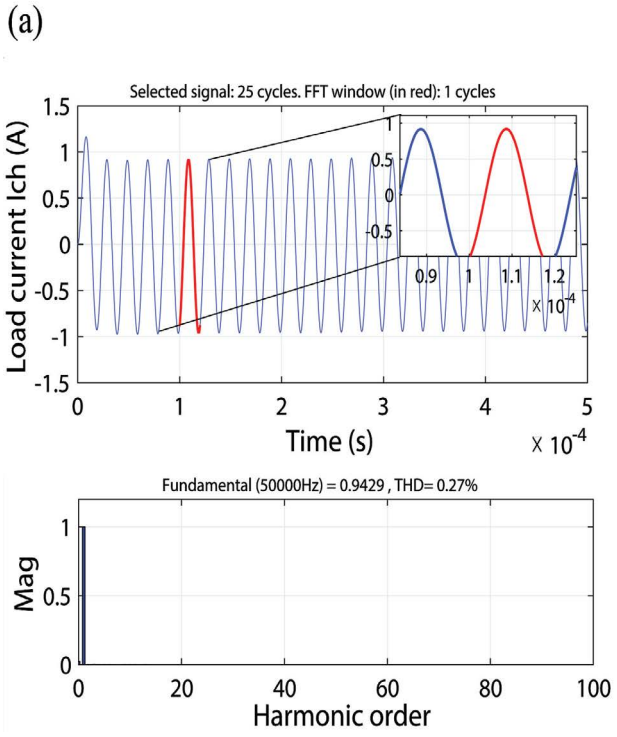

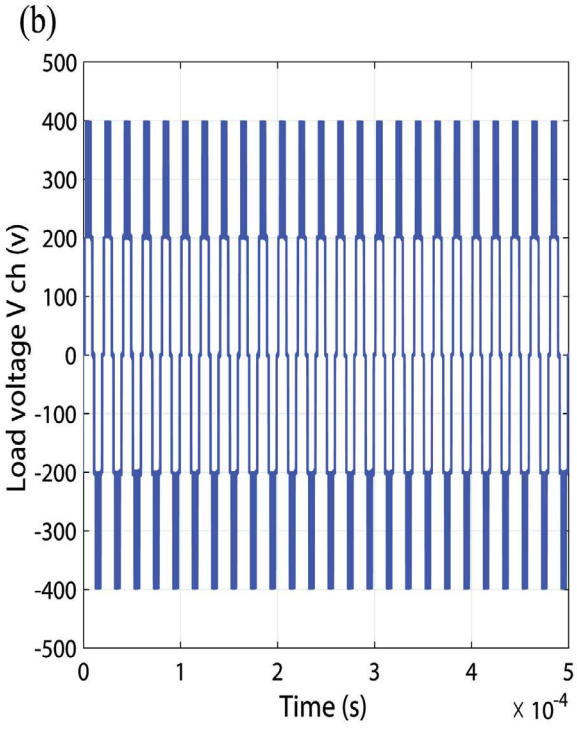

Fig. 6. Discharge lamp: (a) load current with its harmonic spectrum and (b) load voltage.

The shapes of these signals are sinusoidal at a frequency corresponding to the frequency of the modulating signal (50 kHz). With a distortion rate smaller than 0.20%, the proposed system can be considered highly accurate for usages in conventional systems.

At this stage in the open-loop system and without consideration of temperature perturbation, we report the root mean square (RMS) arc current in Fig. 8.

We see in Fig. 8 that, even without external perturbations, the RMS arc current presents a transient initial peak of about 15% of the final response and possesses a nominal value around I_{arc} = 0.65 A, associated with undulations, and a long-term permanent decrease as enlightening in the insert of the figure. This observation naturally leads us to consider a closed-loop control system, as we will see in the next part of this contribution, and for the regulation, we have chosen to develop an efficient based proportional-integral control system.

2.5. Simulation of the discharge lamp-electronic ballast system in closed-loop

As seen above, to improve the performance of the discharge lamp on the radiation plane, we must maintain the RMS arc current of the lamp rigorously steady around a constant value close to 0.65 A. Thus, we introduce a PI regulator of the arc current [27]. The block diagram of the PI controller is illustrated in Fig. 9.

$C(s) = K_p + K_i/s$ is the transfer function of the proportional-integral controller, K_p and K_i are the controller gains calculated using the pole placement method. The well-known transfer function of the close loop regulator is given by:

$$\text{CLTF} = \frac{C(s)\cdot G(s)}{1 + C(s)\cdot G(s)} \tag{14}$$

where $G(s)$ is the transfer function of the open-loop system.

With this closed-loop regulation system, after simulation, we have found a total harmonic distortion, THD of the load current equal to 0.09% hugely improved compared to the THD found for the open-loop system.

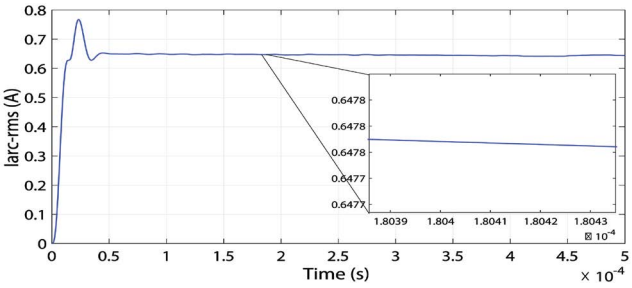

Fig. 8. Discharge lamp RMS arc current.

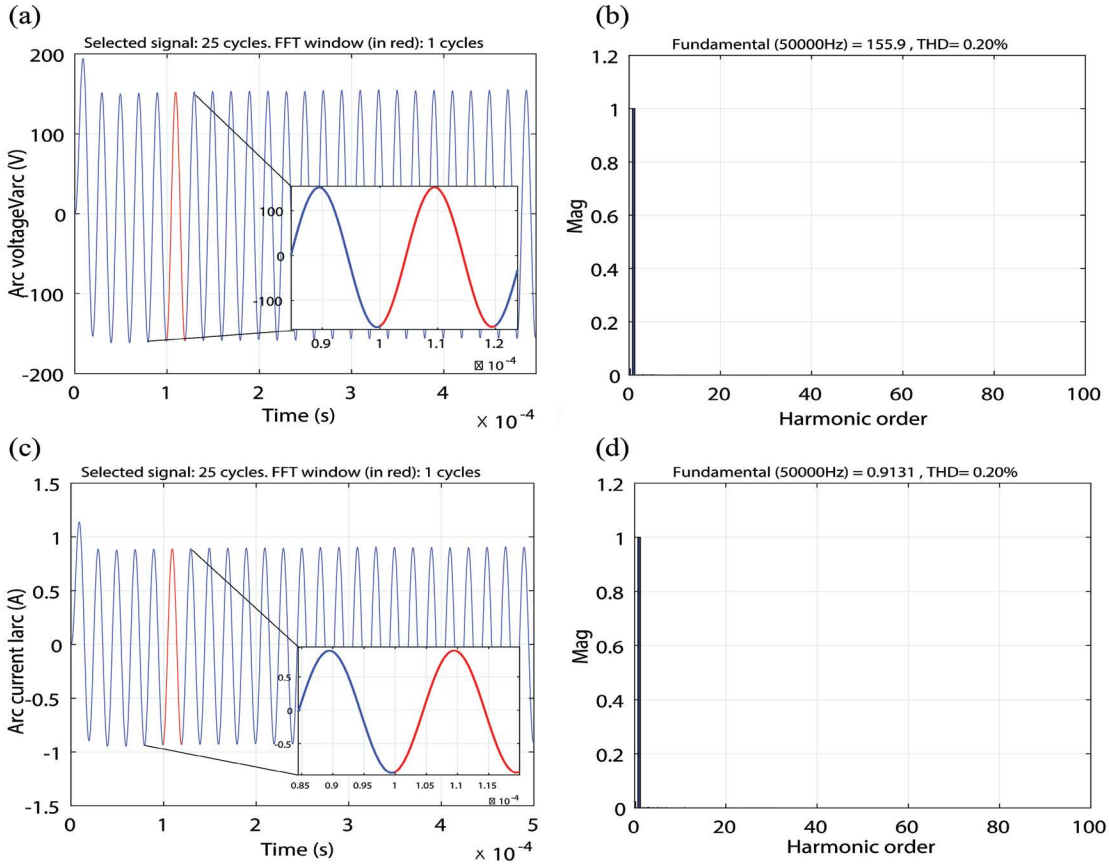

Fig. 7. Discharge lamp: (a and b) arc voltage, (c and d) arc current with their harmonics spectra.

The resulting arc voltage and current are represented in Fig. 10 and the RMS arc current of the lamp in Fig. 11.

As shown in Fig. 10 the final THD of the arc current achieved a very low level equal to 0.04%, to be compared to the first value of the THD, equal to 0.20% achieved with the previous basic open-loop system. Finally, we can notice in Fig. 11 the disappearance of the transient initial peak current, and the RMS arc current perfectly stabilized around the nominal functioning point of 0.65 A without fluctuations in the steady-state.

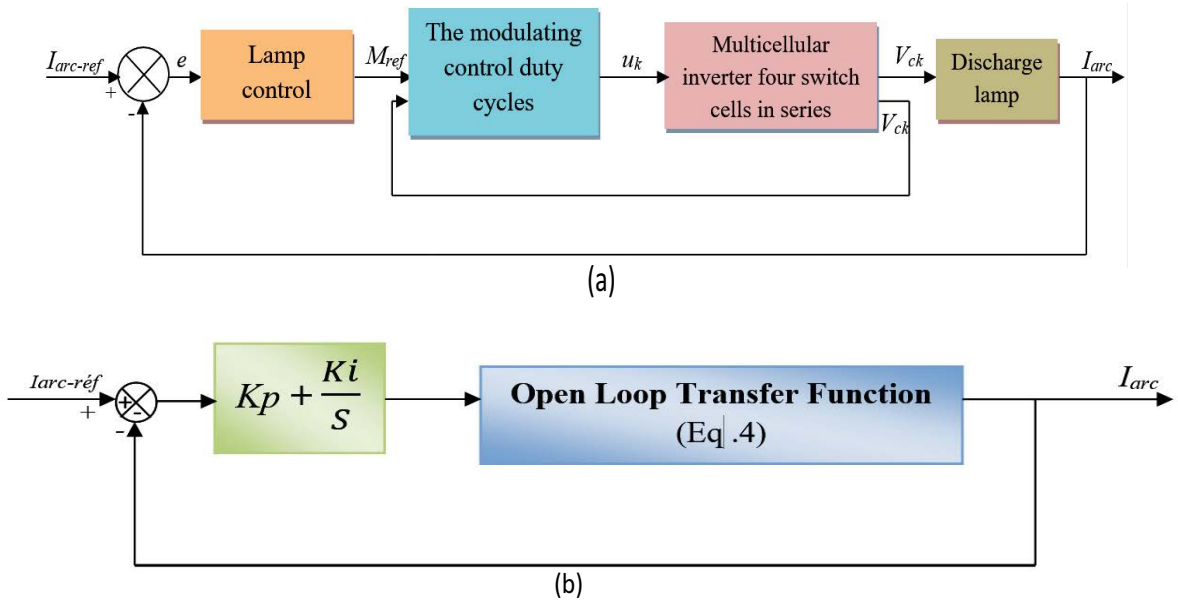

Fig. 9. (a) Block diagram of the control of the discharge lamp with a control modulating duty cycles for the inverter and (b) control loop system with PI controller.

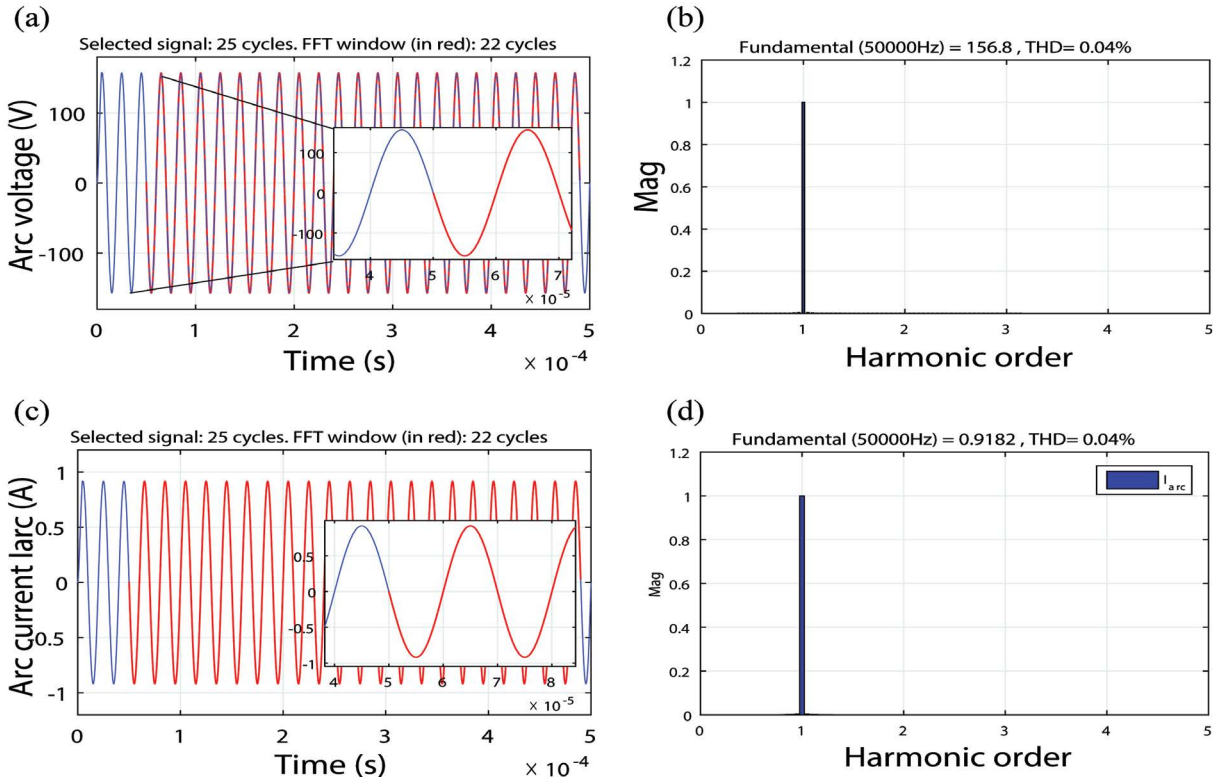

Fig. 10. (a and b) Arc voltage, (c and d) arc current and their harmonic spectrum of the system with PI controller.

2.6. Robustness of discharge lamp-electronic ballast system in closed-loop

It is well-known that the main interest of a closed-loop regulation is the improvement of the robustness of the controlled system. Thus, in what follows, we test the capability of our closed-loop controller to regulate the supply of the UV lamp when the functioning temperature changes. The variation of this temperature induces changes of the arc resistance, which is inversely proportional to the arc current variations [11].

To test the robustness of the system, we have considered an extreme case with a temperature perturbation corresponding to a step of 40% of the initial value at a simulating time of 10^{-4} s.

We represent in Figs. 12 and 13, the flying capacitor voltages and arc voltage and current V_{arc} and I_{arc} and report in Fig. 14 the RMS arc current, after a disturbance of 40% appearing at 10^{-4} s in the simulation cycle.

It is to be noted that we have considered a perturbation induced by an instantaneous increase of the temperature with a step equal to 40% of its initial value. Thus, the chosen value for this perturbation corresponds to a pure simulation approach allowing the test of the system performance taking into account all possible disturbances in practice and by testing the operation of the control system within its own operating limits.

Thus, we see in Fig. 12 that the perturbation of the system induces a high stability of the flying capacitor voltages, rapidly recover after the disturbance but with new constant levels increase at around 25%. Concerning the functioning conditions of the lamp after the perturbations, we notice, Fig. 13, that after the temperature disturbance, the arc voltage decreases by 54% whereas the arc current is instantaneously stabilized at its nominal value. The phenomenon link to the voltages, that is, the raising of the flying capacitor voltages and the decrease of the arc voltage, can be considered as the main limitation of the PI regulation based on the currents as it can induce over-voltages on the switches and the capacitors, and a decrease of the arc power. Nevertheless, as reported in Fig. 14, we see that the RMS arc current finds its nominal value after 30 µs thanks to the PI controller. This high stability of the current corresponds to the objectives which were fixed initially in this work and it shows that the regulator PI is a performing solution in the supply of UV lamps destined to the treatment of waters when the components of the power supply, as capacitors, are sized to support high voltages. Compared to the electrical current delivered with a power supply functioning in an open-loop, that corresponding to the starting point of this study, the stability of the arc current achieved with a multicellular converter associated with a closed-loop PI regulation will ensure a better UV-C generation at 253.7 nm,

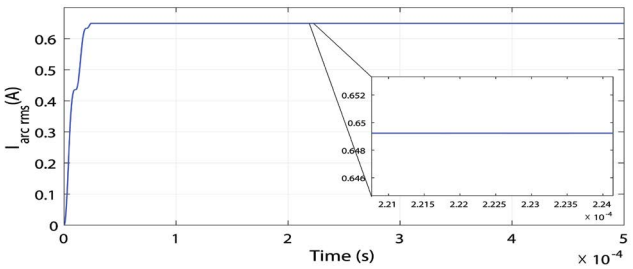

Fig. 11. RMS arc current of the lamp with a PI regulator.

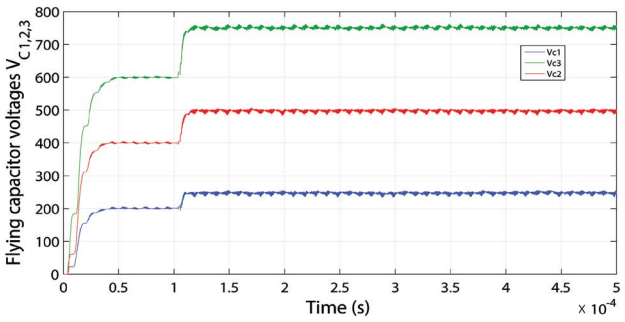

Fig. 12. Flying capacitor voltages V_{c1}, V_{c2}, V_{c3} (v) after a disturbance of 40% at 10^{-4} s.

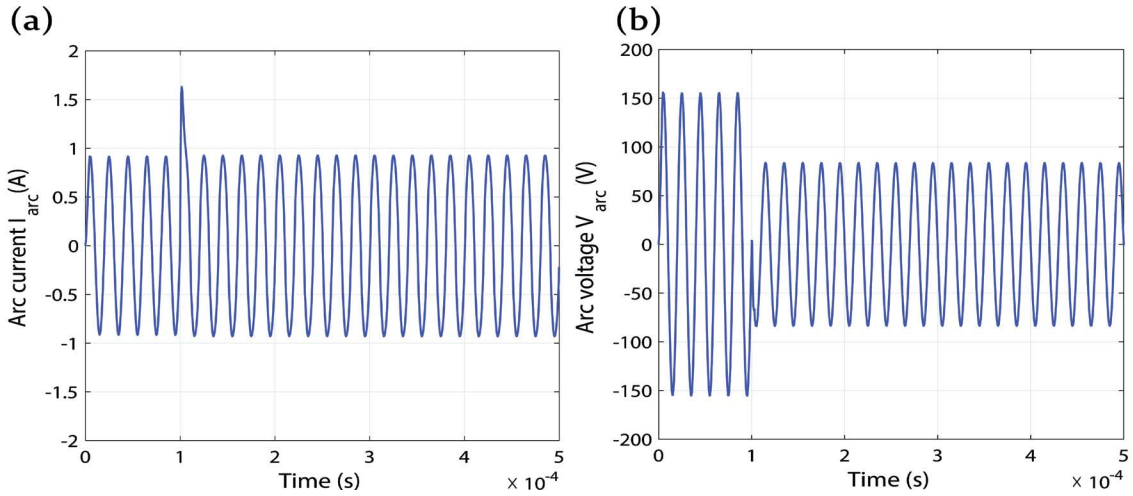

Fig. 13. Arc voltage and current V_{arc} and I_{arc} after a disturbance of 40% at 10^{-4} s.

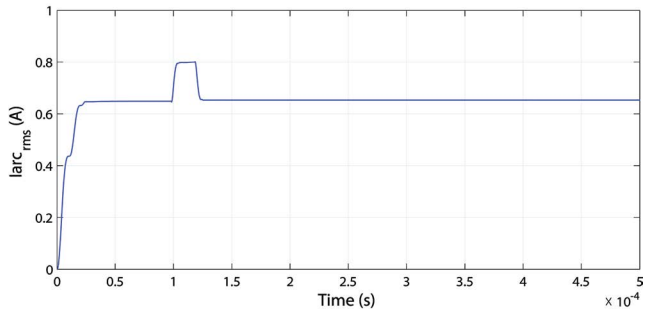

Fig. 14. RMS arc current $I_{\text{arc-RMS}}$ after a disturbance of 40% at 10^{-4} s.

therefore a better efficiency of the tertiary treatment of the micro-organism pathogens in the water and also will ensure an increase in the lifetime of the lamp which is a functional and economic factor not to be neglected.

3. Conclusion

This study has proposed the supply of an electronic ballast-discharge lamp system by a multicellular converter (4 cells in series) for water disinfection. Multicellular series converter has been widely discussed namely its functioning, its modeling and its control. The modulating duty cycles was established for controlling the capacitor voltages in order to ensure the balancing voltages across the power switches. To improve the lifetime and the efficiency of the discharge lamp, that is, a stabilized radiation emission at 253.7 nm assuming a better efficiency of the tertiary treatment of the microorganism pathogens in the water, the maintain at 0.65 A_{rms} the arc current must be strictly achieved. This fact imposes a current regulation here assumes by a classic PI type regulator. This regulator was modeled by the pole placement method and simulated using MATLAB/SimPower. Tested in a worst perturbing case, that is, with an instantaneous increase of 40% of the water temperature, this topology based on a multicellular converter associated with a closed-loop PI regulation assumes a good control of the arc current despite the presence of a disturbance on the arc current and parametric variations on the arc resistance. Finally, the results obtained in this paper confirm the choice of a multicellular converter for supplying a discharge lamp. The next step to be considered should be the hardware implementation.

Acknowledgments

We are grateful to Jean-Pierre Charles, Emeritus Professor, University of Lorraine and Centrale Supelec (France) for his essential participation in this research and the useful scientific discussions and constructive criticisms on this specific subject.

References

[1] L.A. De Oro, G. De A. Melo, C.A. Canesin, UV Dose Investigation for Imersed Lamp Purifier for Electronic Ballast UV Lamps Design, 16th International Power Electronics and Motion Control Conference and Exposition (PEMC), IEEE, Antalya, Turkey, September 2014, pp. 893–900.

[2] D. Vaju, C. Festila, G. Vlad, Drinking Water Quality Improvement by Physical Methods, Using Middle-Frequency Inverters, International Conference on Automation, Quality and Testing, Robotics (AQTR), Cluj-Napoca, Romania, 22–25 May 2008, pp. 454–459.

[3] A. Grimes, N. Migliore, M. Mitchell, J. Sweetgall, Effects of Portable, Manually Powered Ultra-violet Water Treatment, IEEE 35th Annual Northeast Bioengineering Conference, IEEE, Cambridge, MA, USA, 2009, pp. 1–2.

[4] J. Willy Masschelein, Utilisation des U.V. dans le traitement des eaux: Use of U.V. in water treatment, Editeur Ed. Cebedoc, 2000, 109 p.

[5] L. Bouslimi, A. Chammam, M. Ben Mustapha, M. Stambouli, J.P. Cambronne, Simulation and Experimental Study of an Electronic Pulsed Power Supply for HID Lamps Intended for Photochemical Applications, International Review of Electrical Engineering (IREE), Vol. 4, No. 5, Part A, (September–October 2009), pp. 799–808, ISSN 1827–6660.

[6] A. Djuretic, M. Kostic, Comparison of electronic and conventional ballasts used in roadway lighting, Light. Res. Technol., 46 (2014) 407–420.

[7] E. Persson, K. Dong, A Performance Comparison of Electronic vs. Magnetic Ballast for Powering Gaz – Discharge UV Lamps, Nicollet Technologies Corporation, Presented at Red Tech'98, Chicago, USA.

[8] A. Aissa-Bokhtache, Commande d'un système lampe à décharge-Ballast électronique pour épuration des eaux: Control of a Discharge Lamp-Electronic Ballast System for Water Purification, Magister Thesis, Hassiba Ben Bouali University Chlef, 2005.

[9] A. Aissa-Bokhtache, A. Zegaoui, M. Kellal, M.S. Boucherit, B. Belmadani, M. Aillerie, Optimization based on fuzzy logic control of discharge lamp-electronic ballast system for water purification, Electr. Power Compon. Syst., 44 (2016) 1981–1990.

[10] A. Aissa-Bokhtache, A. Zegaoui, B. Belmadani, M.S. Bouchrit, Water purification by a lamp discharge-electronic ballast system using a full bridge inverter, Energy Procedia, 74 (2015) 446–452.

[11] S. Harley, B. Schuba, D. Corkal, Ultraviolet Disinfection of Private Water Supplies for House Hold or Agricultural Uses, Agriculture and Agri-Food Canada, November 2008.

[12] C. Costache Mongrand, J.J. Damelincourt, G. Zissis, Optimisation d'une source d'ultraviolet fonctionnant dans un réacteur de traitement d'eau de consommation: Optimisation of an ultraviolet source working in a consumer water reactor, UVX 2000 Colloque sur les sources cohérentes et incohérentes UV, VUV, et X – Applications et développements récents No. 5, Ile de Porquerolles, Vol. 87, pp. Pr7.65–Pr7.66, France, 2001.

[13] A. Toumi, L. Chhun, S. Bhosle, G. Zissis, P. Maussion, J. Hirsch, Acoustic Resonance Characterization and Numerical Model Including Acoustic Streaming in an HPS Lamp, Vol. 49, IEEE Industry Applications Society Annual Meeting, IEEE, Orlando, FL, USA, 2013, pp. 1154–1160.

[14] S. Mariethoz, A.C. Rufer, Design and control of asymmetrical multilevel inverters, IECON 02, November 2002, doi: 10.1109/IECON.2002.1187617.

[15] C.S. Moo, H.C. Yen, Y.C. Hsieh, C.R. Lee, A Fluorescent Lamp Model for High-Frequency Electronic Ballasts, Vol. 5, Conference Record of the 2000 IEEE Industry Applications Conference, Thirty-Fifth IAS Annual Meeting and World Conference on Industrial Applications of Electrical Energy (Cat. No.00CH37129), IEEE, Rome, Italy, 2000, pp. 3361–3366.

[16] H.C. Yen, Z.J. Huang, K.H. Lee, Fluorescent Lamp Model for High-Frequency Electronic Ballasts, International Conference on Power Electronics and Drives Systems (PEDS), Kuala Lumpur, Malaysia, 28 Nov.–1 Dec. 2005, pp. 1184–1189.

[17] H.C. Yen, Z.J. Huang, K.H. Lee, A Fluorescent Lamp Model for High-Frequency Electronic Ballasts, Industry Applications Conference, Conference Record IEEE, Vol. 2, November 2005, pp. 1184–1189.

[18] L. Amet, M. Ghanes, J.P. Barbot, Direct Control Based on Sliding Mode Techniques for Multicell Serial Chopper, Proceedings

of the 2011 American Control Conference (ACC), IEEE, San Francisco, CA, USA, 2011, pp. 751–756.
[19] R. Banaei Mohamad, J. Oskuee, Mohajel, F.M. Kazemi, A new advanced topology of stacked multicell inverter, Int. J. Emerg. Electric Power Syst., 15 (2014) 327–333.
[20] D. Pinon, M. Fadel, H. Meynard, Sliding mode control for a two-cell chopper: study of the convergence to limit cycle, Rev. Int. Gen. Elect., 1 (1998) 393–415.
[21] F. Defay, A.-M. Llor, M. Fadel, A predictive control with flying capacitor balancing of a multicell active power filter, IEEE Trans. Ind. Electron., 55 (2008) 3212–3220.
[22] P. Carrere, Etude et réalisation des convertisseurs multicellulaires série à IGBT: Study and realization of multicellular serial to IGBT converters, Doctorat Thesis, National Polytechnic, Institute of Toulouse (INPT), 1996.
[23] L. Göhler, H. Wenner, K. Klaus, A United Compact Model for Depletion MOSFETs in Smart Power applications, Rev. IEEE, 2000.
[24] O. Tachon, M. Fadel, T. Meynard, Control of series multicell converters by linear state feedback decoupling, EPE'97, 7th European Conference on Power Electronics and Applications, Brussels, Belgium, 1997, pp. 1588–1593.
[25] M. Aimé, G. Gateau, M. Fadel, Commande des convertisseurs multi cellulaires série à fréquence fixe en mode courant: Control of serial multi-cellular converters at fixed frequency in current mode, CIFA'04, Douz, (Tunisie), 22–24 Nov. 2004.
[26] C.S. Helder, A. Corrêa Pinto Joào, A.A. Ernane, Cœlho, L.H.S.C. Barreto, J.F. Luizc de Freitas, J.R. Valdier, JoàoVieira, High Power Factor Electronic Ballast for Tubular Fluorescent Lamp, Universidade Federal de Vbalândice, Faculdade de engenharia electricaFeelt campus, Santa Monica, Brazil, Rev. EPE, 2001.
[27] J.M. Flaus, La régulation industrielle, régulateur PID, prédictifs et flous: Industrial regulation, PID regulator, predictive and fuzzy, Traité des nouvelles technologies, Série automatique, Edition Hermes, Paris, 1994.